Version 01 as of December 9, 2019
Primary authors: Carlos Yero, Werner Boeglin, Mark Jones
To be submitted to PRL
Comment to cyero002@fiu.edu by xxx, yyy
DØ INTERNAL DOCUMENT – NOT FOR PUBLIC DISTRIBUTION

First Measurements of the D(e,e'p)n Cross Section at Very High Recoil Momenta and Large Q^2

C. Yero and W.U. Boeglin
Florida International University, University Park, Florida 33199, USA

M.K. Jones
Thomas Jefferson National Accelerator Facility,
Newport News, Virginia 23606, USA

(for the Hall C Collaboration)

(Dated: December 9, 2019)

Abstract

New ${}^2H(e,e'p)n$ cross sections have been measured at 4-momentum transfers $Q^2 = 4.5 \pm 0.5$ (GeV/c)^2 for neutron recoil (missing) momenta up $p_r \sim 1.18$ GeV/c at several fixed neutron recoil angles (θ_{nq}) with respect to the 3-momentum transfer, $\vec{q}$. At neutron angles of 35 and 45 degrees final state interactions (FSIs) as well as meson exchange currents (MECs) and isobar configurations (ICs) are expected to be suppressed and the plane wave impulse approximation (PWIA) provides the dominant cross section contribution. The new data are compared to recent theoretical calculations where significant disagreement at very high missing momenta has been observed.

Being the only two-nucleon bound system, the deuteron serves as a starting point to study the strong nuclear force at the subfermi distance scale, a region which is currently not well understood. At such small inter-nucleon distances the NN (nucleon-nucleon) potential is expected to exhibit a repulsive core in which the interacting nucleon pair begins to overlap. The overlap is directly related to two-nucleon short range correlations

(SRC) observed in $A > 2$ nuclei [1–4]. Short-range studies of the deuteron are also important in determining whether or to what extent the description of nuclei in terms of nucleon/meson degrees of freedom is still valid before having to include explicit quark degree of freedoms, an issue of fundamental importance in nuclear physics[5]. As of the present time, there are only a few nuclear physics experiments for which a transition between nucleonic to quark degrees of freedom been observed [6–8].

The most direct way to study the short range structure of the deuteron wavefunction (or equivalently, its high momentum components) is via the exclusive deuteron electro-disintegration reaction at very high neutron recoil (or missing) momenta. Within the PWIA the virtual photon couples to the proton which is subsequently ejected from the nucleus without further interaction with the recoiling neutron, which carries a momentum equal in magnitude but opposite in direction to the initial state proton, $\vec{p}_r = -\vec{p}_{i,p}$, thus providing information on the momentum of the bound nucleon and its momentum distribution.

In reality, the ejected particles undergo subsequent interactions resulting in re-scattering between the proton and neutron (FSIs). Another possibility is that the photon may couple to the virtual meson being exchanged between the nucleons (MECs), or the photon may excite either nucleon in the deuteron into a resonance state (ICs) which decays back into the ground state nucleon causing further re-scattering between the proton and neutron. Both MECs and ICs in addition to FSIs can significantly alter the recoiling neutron momentum thereby obscuring any possibility of directly accessing the deuteron momentum distributions.

Theoretically, MECs and ICs are expected to be suppressed at $Q^2 > 1$ (GeV/c)^2) and Bjorken $x_{Bj} \equiv Q^2/2M_p\omega > 1$, where M_p and ω are the proton mass and photon energy transfer, respectively. The suppression of MECs can be understood from the fact that the estimated MEC scattering amplitude is proportional to $(1+Q^2/m_{meson}^2)^{-2}(1+Q^2/\Lambda^2)^{-2}$, where $m_{meson} \approx 0.71$ (GeV/c)^2 and $\Lambda^2 \sim 0.8 - 1$ (GeV/c)^2[9]. The ICs can be suppressed kinematically by selecting $x_{Bj} > 1$, where one probes the lower part of the deuteron quasi-elastic peak which is maximally away from the inelastic resonance electro-production threshold.

For FSIs at large Q^2, the onset of the General Eikonal Approximation (GEA)[9–11] is expected which predicts a strong angular dependence of the FSIs with neutron recoil angles where FSI peaks at $\theta_{nq} \sim 70^o$. The most important prediction from GEA, however, is that at large recoil momenta p_r where FSIs are expected to be large, there is an approximate cancellation of the PWIA/FSI interference (screening term) with the modulus-squared of the FSI amplitude (rescattering term). This cancellation results in only the PWIA term remaining in the deuteron cross section and is expected to occur at netron recoil angles $\theta_{nq} \sim 40^o$ and $\theta_{nq} \sim 120^o$, opening a kinematic window to study the short-range structure of the deuteron.

Previous deuteron electro-disintegration experiments performed at Jefferson Lab (JLab) have helped confirmed various of the abovementioned theoretical predictions as well as constrain and quantify the contributions from FSIs, MECs and ICs on the $^2H(e, e'p)n$ cross-section to determine the kinematics at which they are either suppressed (MECs and ICs) or under control (FSIs). The first of these was performed in Hall A [12] at a relatively low momentum transfer of $Q^2 = 0.665$ (GeV/c)^2 and neutron recoil momenta up to $p_r = 550$ MeV/c where it was shown that for $p_r > 300$ MeV/c, FSIs, MECs and ICs dominate the cross section and had to be included in Arenhövel's calculations [13–16] for a satisfactory agreement between theory and data.

The next experiment was performed in Hall B [17] using the CEBAF Large Acceptance Spectrometer (CLAS) which measured a wide variety of kinematic settings giving an overview of the $^2H(e, e'p)n$ reaction kinematics. This was the first experiment to probe the deuteron at high momentum transfers ($1.75 \leq Q^2 \leq 5.5$ (GeV/c)^2) and presented angular distributions of cross-sections that exhibited a strong angular dependence of FSI with neutron recoil angles peaking at $\theta_{nq} \sim 70^o$ which confirmed the onset of the GEA[9, 10]. The cross sections versus neutron recoil momenta up to p_r ∼2 GeV/c were also presented, however, statistical limitations made it necessary to integrate over a wide angular range making it impossible to control contributions from FSIs, MECs and ICs.

Finally, a third $^2H(e, e'p)n$ experiment was performed in Hall A [18] at $Q^2 = 3.5 \pm 0.25$ (GeV/c)^2 and recoil momenta up to 550 MeV/c. The angular distributions of the cross-section ratio ($R = \sigma_{exp}/\sigma_{PWIA}$) presented confirmed the strong anisotropy of FSIs with recoil angle θ_{nq} also observed in Hall B[17]. Most importantly, for recoil neutron momentum bins, $p_r = 0.4 \pm 0.02$ and 0.5 ± 0.02 GeV/c, the ratio was found to be $R \sim 1$ for $35^o \leq \theta_{nq} \leq 45^o$ indicating a reduced sensitivity of the experimental cross-section to FSIs. This kinematic window allowed for the first time the extraction of momentum distributions for neutron recoil momenta up to p_r ∼550 MeV/c.

The experiment presented on this Letter takes advantage of the kinematic window previosuly found in Hall A[18] and extends the ${}^2H(e,e'p)n$ cross section measurements to $Q^2 = 4.5 \pm 0.5$ (GeV/c)^2 and neutron recoil momenta up to 1.18 GeV/c. At these kinematics, MECs and ICs are suppressed and FSIs are under control for neutron recoil angles between 35 and 45 degrees giving access to unprecedented high momentum components of the deuteron wavefunction.

This experiment was part of a group of four experiments that commissioned the new Hall C Super High Momentum Spectrometer (SHMS) as part of the 12 GeV upgrade at JLab. A 10.6 GeV electron beam was incident on a 10 cm long liquid deuterium target (LD2). The scattered electron and knocked-out proton were detected in coincidence by the SHMS and the High Momentum Spectrometer (HMS), respectively. The "missing" (undetected) neutron was reconstructed from energy-momentum conservation laws: $\vec{p_r} = \vec{q} - \vec{p_f}$ (missing momentum) and $E_m = \omega - T_p - T_r$ (missing energy), where $\vec{p_f}$ is the final proton momentum, (T_p, T_r) are the final proton and neutron kinetic energies, and E_m is the binding (missing) energy of the deuteron. The beam currents delivered by the accelerator ranged between 45-60 μA and the beam was rastered over a 2x2 mm^2 area to reduce the effects of localized boiling on the cryogenic targets (hydrogen and deuterium).

Both spectrometers at Hall C have similar standard detector packages, each with 1) four sets of hodoscope planes[19] (scintillator arrays) used for triggering, 2) a pair of drift chambers[20] used for tracking, 3) a calorimeter[21] used for e^-/π^- discrimination and 4) a gas Čerenkov [22, 23] used also for e^-/π^- separation. Due to the absence of significant background on this experiment and the low coincidence trigger rates ($\sim 1-3$ Hz) at the higher missing momentum settings, the use of additional particle identification (PID) was found to have little to no effect on the final cross section.

We measured three central missing momentum settings: $p_r = 80, 580$ and 750 MeV/c. At each of these settings, the electron arm (SHMS) was fixed and the proton arm (HMS) was rotated from smaller to larger angles corresponding the the lower and higher missing momentum settings, respectively. At these kinematics, the 3-momentum transfer covered a range of $2.4 \lesssim |\vec{q}| \lesssim 3.2$ GeV/c which is more than twice the highest neutron recoil momentum (p_r) measured on this experiment. As a result one can infer that most of the virtual photon momentum is transferred to the proton which scatters at angles relative to $\vec{q}$ in the range $0.4^o \lesssim \theta_{pq} \lesssim 21.4^o$. At these forward angles and large momentum transferred to the proton, the additional process in which the recoiling neutron is struck by the vitrual photon is suppressed.

Hydrogen elastic ($^{1}H(e, e'p)$) data was also taken at kinematics close to the deuteron p_r=80 MeV setting for cross-checks with the spectrometer acceptance model using the Hall C Monte Carlo simulation program, SIMC. Additional $^{1}H(e, e'p)$ data were also taken at three other kinematic settings that covered the SHMS momentum acceptance range for the deuteron and were used for spectrometer optics optimization, momentum calibration and the determination of the spectrometer offsets and kinematic uncertainties[24, 25].

Identical event selection criteria were used for the hydrogen and deuteron data. The criteria were determined by making 1) standard cuts on the spectrometer momentum fraction (δ) to select a region in which the reconstruction optics is well known, 2) a cut to restrict the HMS solid angle acceptance to events that passed directly through the collimator and not by re-scattering from the collimator edges, 3) a missing energy cut (peak $\sim$ 2.22 MeV for the deuteron) to select true $^{2}H(e, e'p)n$ coincidences, 4) a coincidence time cut to select true coincidence events and not accidentals, 5) a PID cut on the SHMS calorimeter to select electrons and not other sources of background, mostly pions and 6) a cut on the reconstructed HMS and SHMS reaction vertices to select events that truly originated from the same reaction vertex at the target.

The experimental data yield for both hydrogen and deuteron data was normalized by the total charge and corrected for various inefficiencies. For $^{2}H(e, e'p)n$ the corrections were as follows: tracking efficiencies (98.9%-HMS, 96.4%-SHMS), total live time (92.3%), proton loss due to nuclear interactions in the HMS (4.7%)[26] and target boiling factors (4.2%)[27].

For $^{1}H(e, e'p)$, the corrected data yield was compared to SIMC using J. Arrington's proton form factor parametrization[28] to check the spectrometer acceptance model. The ratio of data to simulation yield was determined to be $97.6 \pm 0.3\%$. For $^{2}H(e, e'p)n$, the low missing momentum data (p_r = 80 MeV/c) were compared to the Hall A data (See Fig. 1). The good agreement gives us confidence on the measurements made at higher missing momentum settings for which no previous data exist.

The systematic uncertainties on the measured cross sections were determined from normalization[29] and kinematic uncertainties in the beam energy and spectrometer angle/momentum settings. The individual contributions from normalization uncertainties were determined to be: tracking efficiencies (0.40%-HMS, 0.59%-SHMS), target boiling (0.39%), total live time (3.0%) and total charge (2.0%) for an overall normalization uncertainty added in quadrature of 3.7%.

The systematic uncertainties due to our limited knowledge of the beam energy and spectrometer angle/momentum settings were determined point-to-point in (θ_{nq}, p_r) bins for each data set independently, and added in quadrature for overlapping p_r bins of different data sets. For θ_{nq} = 35, 45 and 75 deg (presented on this Letter) the overall kinematic uncertainty varied up to 6.5% for $p_r \leq 1.01$ GeV/c. The overall systematic uncertainty in the cross section was determined by the quadrature sum of the normalization and kinematic uncertainties. This result was then added in quadrature to the statiscial uncertainty(25-30% on average) to obtain the final uncertainty in the cross section.

The data were radiatively corrected for each bin in (θ_{nq}, p_r) by multiplying measured cross sections to the ratio of the SIMC yield without and with radiative effects. For each bin in (θ_{nq}, p_r), the averaged $^2H(e, e'p)n$ kinematics has also been calculated. The ratio between the calculated cross section at the averaged kinematics and the averaged cross section for this bin has also been determined and used to compare theoretical models to the experimental cross sections. The calculations were based on the Laget model including FSI[30, 31].

Both experimental and theoretical reduced cross sections were extracted from the measured (or model) cross sections for each data set independently and were averaged for overlapping bins in p_r. The reduced cross sections are defined as follows:

$$\sigma_{red} \equiv \frac{\sigma_{exp(th)}}{K f_{rec} \sigma_{cc1}} \qquad (1)$$

where $\sigma_{exp(th)}$ is the 5-fold experimental (or theoretical) differential cross section $\frac{d^5\sigma}{d\omega d\Omega_e d\Omega_p}$, K is a kinematical factor, f_{rec} is the recoil factor that arises from the integration over missing energy and σ_{cc1} is the de Forest[32] electron-proton offshell cross section calculated using the form factor parametrization of Ref.[28]. Within the PWIA, σ_{red} corresponds to the proton momentum distribution inside the deuteron.

Figure 1 shows the extracted experimental and theoretical reduced cross sections as a function of neutron recoil momentum p_r for three angular settings at $Q^2 = 4.5 \pm 0.5$ (GeV/c)^2. The data is compared to the results from the previous Hall A experiment[18] at a $Q^2 = 3.5 \pm 0.25$ (GeV/c)^2. The overlay of the Hall A data (cyan) in Fig. 1 provides a continutity to the data from this experiment in the transition from low (80 MeV/c) to high (580, 750) MeV/c missing momentum settings in which there was no data. There is also an overall good agreement between the two experiments in the regions in which they overlap in p_r.

At larger neutron recoil angles of $\theta_{nq} \sim 75^o$ [Fig. 1(c)], the data follows the CD-Bonn PWIA (momentum distributions) up to p_r ∼100 MeV/c, and at $p_r \gtrsim$300 MeV/c, the FSIs become the dominat process and exhibit a smaller falloff with p_r which obscures any possibility of extracting the momentum distributions. This behaviour of FSI with larger recoil angles was predicted by the GEA[9, 10] and was verified in previous experiments[17, 18]. This experiment kinematics moves away from larger recoil angles and focuses on fowards angles at $\theta_{nq} \sim 40^o$ where the momentum distributions become accessible. As a result, our data at larger recoil angles is statistically limited.

For recoil angles at $\theta_{nq} = 35^o$ and 45^o shown in Figs. 1(a) and 1(b), all models predict similar behaviour of the momentum distribution for recoil momenta up to p_r ∼300 MeV/c which the data verifies. At larger p_r, however, the momentum distributions become increasingly sensitive to the different NN potentials, mainly a difference between the CD-Bonn and either the Paris or AV18 is observed.

In Fig. 1(a) for example, the data is clearly sensitive to the CD-Bonn momentum distributions between recoil momenta of $300 \lesssim p_r \lesssim 750$ MeV/c before transitioning to the Paris/AV18 potentials which is a behaviour that is not well described by any of the models. For recoil angles in Fig. 1(b), a similar behaviour can be observed, as the data is sensitive to the CD-Bonn momentum distributions but only up to $p_r \sim 580$ MeV/c as FSIs start to dominate at lower p_r as opposed to Fig. 1(a). For $p_r > 580$ MeV/c, the data again exhibits a behaviour at the high momentum tails which either the CD-Bonn, Paris or AV18 potentials are unable to describe.

The ratio of the experimental and theoretical reduced cross sections (σ_{red}) to the deuteron momentum distributions (n(p_r)) is shown in Fig. 2. As a reference we selected the deuteron momentum distribution calculated using the charge-dependent Bonn (CD-Bonn) potential[33]. The theoretical calculations for the CD-Bonn and Argonne v_{18} (AV18)[34] potentials were performed by M. Sargsian[35] and those for the Paris potential[31] were done by J.M. Laget[30].

At $\theta_{nq} = 75^o$ [Fig. 2(c)], there is a clear onset of GEA at $p_r \gtrsim 300$ MeV/c where FSI become dominant as indicated by the rise of FSI (solid lines) for all theoretical calculations as compared to the reference. In this region, our experiment is statistically limited as we focused on kinematics at lower recoil angles where FSIs are small. The overlayed Hall A data, however, shows excellent agreement with the Paris FSI. For $p_r < 300$ MeV/c, FSIs are small as indicated by the approximate ratio R$\sim$1 for all the theoretical calculations using FSI, which the data follows. The small dip observed in this region (R<1) is indicative of the approximate cancellation between the PWIA/FSI interference (screening term) and the modulus-squared of FSI (re-scattering) terms in the cross section.

For $\theta_{nq} = 45^o$ [Fig. 2(b)] at $p_r < 300$ MeV/c, all theoretical calculations agree with each other and are sensitive to the momentum distribution inside the deuteron which the data confirms. At $p_r \gtrsim 300$ MeV/c, the Paris/AV18 calculations start to deviate from the CD-Bonn calculations, with the most substantial deviations observed at $p_r \sim 1$ GeV/c. The CD-Bonn calculations are sensitive to momentum distributions up to $p_r \sim$580 MeV/c before FSIs start to dominate (R>1). The data is clearly sensitive to the momentum distributions using the CD-Bonn calculations and show an earlier rise than predicted by theory, a behaviour which is not described by any of the models.

A similar behaviour is observed for $\theta_{nq} = 35^o$ [Fig. 2(a)], where the CD-Bonn calculations are sensitive to momentum distributions up to $p_r \sim 800$ MeV/c before being overwhelmed by FSIs, whereas the Paris/AV18 calculations start to deviate from the CD-Bonn at $p_r \sim 300$ MeV/c. The data shows sensitivity to CD-Bonn momentum distributions up to $p_r \sim$750 MeV/c before transitioning ($R > 1$) to other models.

The $\theta_{nq} = 35^o$ [Fig. 2(a)] is clearly the optimal kinematics to study the high momentum components of the deuteron wavefunction, as the data is sensitive to momentum distributions up to $p_r \sim 750$ MeV/c as compared to $p_r \sim$580 MeV/c for the $\theta_{nq} = 45^o$ setting.

This commissioning experiment extended the previous Hall A cross section measurements on the $^2H(e,e'p)n$ reaction to unprecedented large Q^2 and very high neutron recoil momenta at kinematics that enhanced the high momentum components of the deuteron wavefunction. The experimental reduced cross sections were extracted and found to be best described by M. Sargsian's calculations using the CD-Bonn potential with sensitivity to the momentum distributions up to $p_r \sim 580$ and 750 MeV/c for $\theta_{nq} \sim 45^o$ and 35^o, respectively before the data transitioning to other theoretical models, which is a behavior that was not predicted by any of the models. The early transition observed in both the 35 ad 45 degrees kinematic settings gives a hint that there might be additional degrees of freedom (transition to quark-gluon degrees of freedom) that might not be accounted for in NN potentials presented.

However, given that this experiment ran for only 6 out of the 42 days (21 PAC days assuming 100% beam efficiency) of beam time and 3 out of the 8 kinematic settings approved in the original proposal[36], additional beam time would be required to measure the full kinematic coverage (more missing momentum settings) to gain the necessary statistics in order to make any definitive arguments about the underlying physics observed.

We acknowledge the outstanding support of the staff of the Accelerator and Physics Divisions at Jefferson Lab as well as the entire Hall C staff, technicians, graduate students and users who took shifts or contributed to the equipment for the Hall C upgrade making all four commissioning experiments possible.

[1] K. S. Egiyan *et al.* (CLAS Collaboration), Observation of nuclear scaling in the $A(e,e^{'})$ reaction at $x_B > 1$, Phys. Rev. C **68**, 014313 (2003).

[2] K. S. Egiyan *et al.* (CLAS Collaboration), Measurement of two- and three-nucleon short-range correlation probabilities in nuclei, Phys. Rev. Lett. **96**, 082501 (2006).

[3] R. Shneor *et al.* (Jefferson Lab Hall A Collaboration), Investigation of proton-proton short-range correlations via the $^{12}\mathrm{C}(e,e^{'}pp)$ reaction, Phys. Rev. Lett. **99**, 072501 (2007).

[4] N. Fomin, D. Higinbotham, M. Sargsian, and P. Solvignon, New results on short-range correlations in nuclei, Annual Review of Nuclear and Particle Science **67**, 129159 (2017).

[5] P. Ulmer *et al.*, Short-Distance Structure of the Deuteron and Reaction Dynamics in ^{2}H(e,e'p)n, https://www.jlab.org/exp_prog/proposals/01/PR01-020.pdf (2001), *Jefferson Lab Proposal E01-020*.

[6] C. Bochna *et al.*, Measurements of deuteron photodisintegration up to 4.0 gev, Phys. Rev. Lett. **81**, 4576 (1998).

[7] E. C. Schulte *et al.*, Measurement of the high energy two-body deuteron photodisintegration differential cross section, Phys. Rev. Lett. **87**, 102302 (2001).

[8] E. C. Schulte *et al.*, High energy angular distribution measurements of the exclusive deuteron photodisintegration reaction, Phys. Rev. C **66**, 042201 (2002).

[9] M. M. Sargsian, Selected Topics in High Energy Semi-Exclusive Electro-Nuclear Reactions, International Journal of Modern Physics E **10**, 405457 (2001).

[10] L. L. Frankfurt, M. M. Sargsian, and M. I.

Strikman, Feynman graphs and generalized eikonal approach to high energy knock-out processes, Phys. Rev. C **56**, 1124 (1997).

[11] W. Boeglin and M. Sargsian, Modern studies of the deuteron: From the lab frame to the light front, International Journal of Modern Physics E **24**, 1530003 (2015), https://doi.org/10.1142/S0218301315300039.

[12] P. E. Ulmer *et al.*, $^2\mathrm{H}(e,e'p)n$ reaction at high recoil momenta, Phys. Rev. Lett. **89**, 062301 (2002).

[13] H. Arenhövel, W. Leidemann, and E. L. Tomusiak, Inclusive deuteron electrodisintegration with polarized electrons and a polarized target, Phys. Rev. C **43**, 1022 (1991).

[14] H. Arenhövel, W. Leidemann, and E. L. Tomusiak, Exclusive deuteron electrodisintegration with polarized electrons and a polarized target, Phys. Rev. C **46**, 455 (1992).

[15] H. Arenhövel, W. Leidemann, and E. L. Tomusiak, Nucleon polarization in exclusive deuteron electrodisintegration with polarized electrons and a polarized target, Phys. Rev. C **52**, 1232 (1995).

[16] H. Arenhövel, F. Ritz, H. Göller, and T. Wilbois, Consistent treatment of relativistic effects in electrodisintegration of the deuteron, Phys. Rev. C **55**, 2214 (1997).

[17] K. S. Egiyan *et al.* (CLAS Collaboration), Experimental study of exclusive $^2\mathrm{H}(e,e'p)n$ reaction mechanisms at high Q^2, Phys. Rev. Lett. **98**, 262502 (2007).

[18] W. U. Boeglin *et al.* (For the Hall A Collaboration), Probing the high momentum component of the deuteron at high Q^2, Phys. Rev. Lett. **107**, 262501 (2011).

[19] G. Niculescu, I. Niculescu, M. Burton, D. Coquelin, K. Nisson, and T. Jarell, Shms hodoscope scintillator detectors, `https://hallcweb.jlab.org/document/howtos/shms_scintillator_hodoscope.pdf`.

[20] M. Christy, P. Monaghan, N. Kalantarians, D. Biswas, and M. Long, Shms drift chambers, `https://hallcweb.jlab.org/document/howtos/shms_drift_chambers.pdf`.

[21] H. Mkrtchyan *et al.*, The lead-glass electromagnetic calorimeters for the magnetic spectrometers in hall c at jefferson lab, Nuclear Instruments and Methods in Physics Research Section A: Accelerators, Spectrometers, Detectors and Associated Equipment **719**, 85100 (2013).

[22] W. Li, *Heavy Gas Cherenkov Detector Construction for Hall C at Thomas Jefferson National Accelerator Facility*, Master's thesis, University of Regina (2012).

[23] D. Day, Preliminary design of the shms noble cerenkov detector, `https://hallcweb.jlab.org/DocDB/`

0009/000933/001/shms-cerv6.pdf.

[24] C. Yero, Update on spectrometer offsets determination using h(e,e'p) elastics (2019), https://hallcweb.jlab.org/DocDB/0010/001036/002/HC_SoftwareMeeting_Oct03_2019_pdf.pdf.

[25] C. Yero, Optics optimization for the d(e,e'p)n experiment [e12-10-003] (2019), https://hallcweb.jlab.org/DocDB/0010/001033/001/d2_optim.pdf.

[26] C. Yero, Proton absorption (2019), https://hallcweb.jlab.org/DocDB/0010/001020/002/ProtonAbsorption_slides.pdf.

[27] C. Yero, Hms target boiling studies (2019), https://hallcweb.jlab.org/DocDB/0010/001023/003/TargetBoiling_v2.pdf.

[28] J. Arrington, Implications of the discrepancy between proton form factor measurements, Phys. Rev. C **69**, 022201 (2004).

[29] Conservative estimates on the systematic uncertainties of the total live and charge were made. Determination of systematics on these quantities is a work in progress. (Private communication with D. Mack).

[30] J. Laget, The electro-disintegration of few body systems revisited, Physics Letters B **609**, 49 (2005).

[31] M. Lacombe, B. Loiseau, J. M. Richard, R. V. Mau, J. Côté, P. Pirès, and R. de Tourreil, Parametrization of the paris $n-n$ potential, Phys. Rev. C **21**, 861 (1980).

[32] T. D. Forest, Off-shell electron-nucleon cross sections: The impulse approximation, Nuclear Physics A **392**, 232 (1983).

[33] R. Machleidt, High-precision, charge-dependent bonn nucleon-nucleon potential, Phys. Rev. C **63**, 024001 (2001).

[34] R. B. Wiringa, V. G. J. Stoks, and R. Schiavilla, Accurate nucleon-nucleon potential with charge-independence breaking, Phys. Rev. C **51**, 38 (1995).

[35] M. M. Sargsian, Large Q^2 electrodisintegration of the deuteron in the virtual nucleon approximation, Phys. Rev. C **82**, 014612 (2010).

[36] W. U. Boeglin *et al.*, Deuteron Electro-Disintegration at Very High Missing Momenta, https://www.jlab.org/exp_prog/proposals/10/PR12-10-003.pdf.

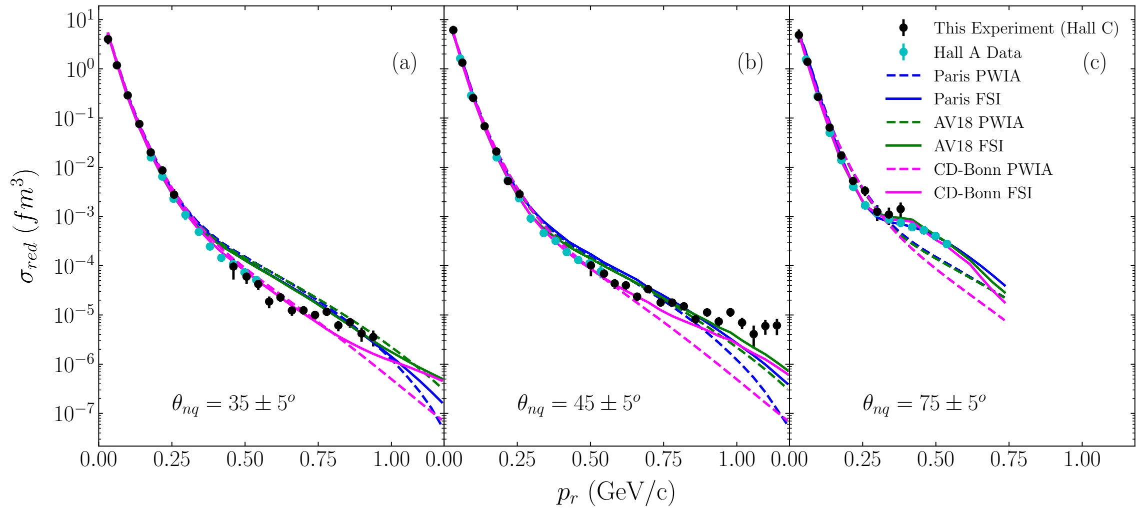

FIG. 1. The reduced cross sections $\sigma_{red}(p_r)$ as a function of neutron recoil momentum p_r are shown in (a)-(c) for recoil angles $\theta_{nq} = 35^o, 45^o$ and 75^o, respectively, with a bin width of $\pm 5^o$. The data is compared to the previous Hall A experiment (cyan) results[18] as well as the theoretical reduced cross sections using the Paris(blue), AV18(green) and CD-Bonn(magenta) NN potentials

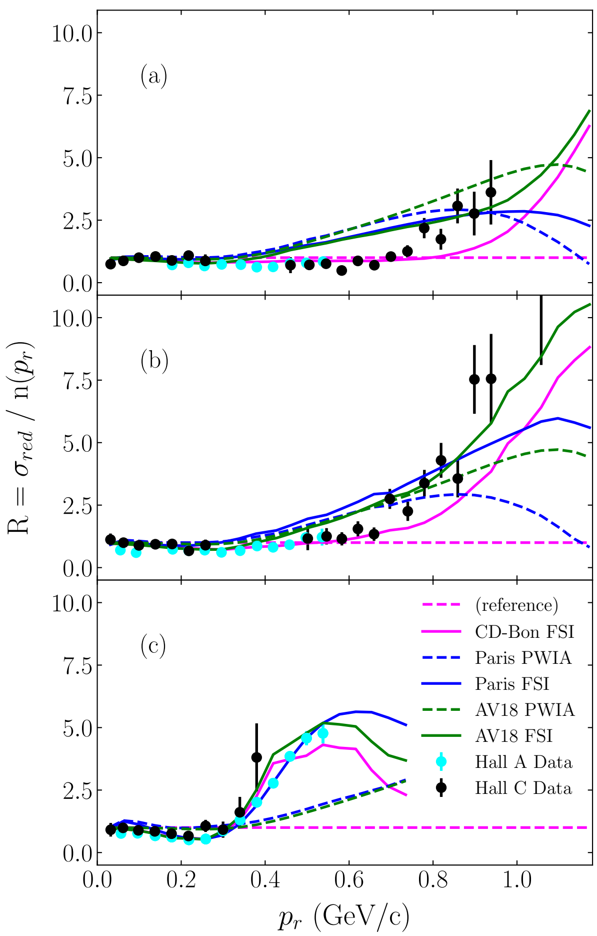

FIG. 2. The ratio $\mathrm{R}(p_r) = \sigma_{red}/\mathrm{n}(p_r)$ is shown in (a)-(c) for $\theta_{nq} = 35^o, 45^o$ and 75^o, respectively, each with a bin width of $\pm 5^o$. The dashed reference (magenta) line refers to CD-Bonn momentum distribution ($\mathrm{n}(p_r)$) by which the data and all models are divided.